frontiers | Frontiers in Energy Research

TYPE Original Research
PUBLISHED 10 March 2023
DOI 10.3389/fenrg.2023.1150000

OPEN ACCESS

EDITED BY
Sara Colussi,
University of Udine, Italy

REVIEWED BY
Alfonso J. Carrillo,
Institute of Chemical Technology (CSIC), Spain
Bamidele Victor Ayodele,
University of Technology Petronas, Malaysia

*CORRESPONDENCE
Kalliopi Kousi,
k.kousi@surrey.ac.uk

†These authors have contributed equally to this work and share first authorship

SPECIALTY SECTION
This article was submitted to Carbon Capture, Utilization and Storage, a section of the journal Frontiers in Energy Research

RECEIVED 23 January 2023
ACCEPTED 20 February 2023
PUBLISHED 10 March 2023

CITATION
Ali SA, Safi M, Merkouri L-P, Soodi S, Iakovidis A, Duyar MS, Neagu D, Reina TR and Kousi K (2023), Engineering exsolved catalysts for CO_2 conversion. *Front. Energy Res.* 11:1150000. doi: 10.3389/fenrg.2023.1150000

Engineering exsolved catalysts for CO_2 conversion

Swali A. Ali[1†], Manzoor Safi[1†], Loukia-Pantzechroula Merkouri[1], Sanaz Soodi[1], Andreas Iakovidis[2], Melis S. Duyar[1], Dragos Neagu[3], Tomas Ramirez Reina[4] and Kalliopi Kousi[1*]

[1]School of Chemistry and Chemical Engineering, University of Surrey, Guildford, United Kingdom, [2]School of Mechanical Engineering Sciences, University of Surrey, Guildford, United Kingdom, [3]Department of Chemical and Process Engineering, University of Strathclyde, Glasgow, United Kingdom, [4]Department of Inorganic Chemistry and Material Sciences Institute of Seville, University of Seville-CSIC, Seville, Spain

Introduction: Innovating technologies to efficiently reduce carbon dioxide (CO_2) emission or covert it into useful products has never been more crucial in light of the urgent need to transition to a net-zero economy by 2050. The design of efficient catalysts that can make the above a viable solution is of essence. Many noble metal catalysts already display high activity, but are usually expensive. Thus, alternative methods for their production are necessary to ensure more efficient use of noble metals.

Methods: Exsolution has been shown to be an approach to produce strained nanoparticles, stable against agglomeration while displaying enhanced activity. Here we explore the effect of a low level of substitution of Ni into a Rh based A-site deficienttitanate aiming to investigate the formation of more efficient, low loading noblemetal catalysts.

Results: We find that with the addition of Ni in a Rh based titanate exsolution is increased by up to ~4 times in terms of particle population which in turn results in up to 50% increase in its catalytic activity for CO_2 conversion.

Discussion: We show that this design principle not only fulfills a major research need in the conversion of CO_2 but also provides a step-change advancement in the design and synthesis of tandem catalysts by the formation of distinct catalytically active sites.

KEYWORDS

carbon dioxide utilisation, exsolution, dry reforming, greenhouse gases, efficient catalysts

1 Introduction

Rapid increase in industrial development and population growth over the last several decades have continuously increased the demand for energy, a key pre-requisite for our lives, subsequently resulting in an increase in green-house gas emissions, particularly CO_2 and CH_4 (Gao et al., 2011; Maestri et al., 2009). An increase of 0.8°C in global surface temperature occurred in 20th century and further surge (1.4°C–5.8°C) has been expected in 21st century (McCarthy et al., 2001). As a result, serious environmental damage has occurred, such as ocean acidification, droughts, hurricanes, and floods (Ainsworth et al., 2008). Therefore, there is a need not only to mitigate climate change, possibly by capture and storage of CO_2, but also to investigate available resources, such biogas, in order to utilize CO_2 and replace chemicals that are fossil fuel derivatives (Naidja et al., 2003; Izquierdo et al., 2013). In this regard, dry reforming of

methane (DRM) (Eq. 1) is a promising potential solution for utilizing two abundantly available greenhouse gases (CO_2 and CH_4) to industrially important syngas (mixture of H_2 and CO) with ratio of 1 to 1 (H_2:CO = 1:1) that can subsequently be used to produce a wide range of products such as higher alkanes and oxygenates *via* Fischer-Tropsch synthesis (Wang et al., 2018; Abdulrasheed et al., 2019; Buelens et al., 2016) or to manufacture fine chemicals *via* hydroformylation reactions (le Saché and Reina, 2022).

$$CH_4 + CO_2 \leftrightarrow 2H_2 + 2CO \quad (\Delta H^o = +247kJ/mol) \qquad (1)$$

In addition, provided that the energy required for conducting the DRM reaction comes from non-hydrocarbon resources, this approach reduces the net emission of greenhouse gases as compared to alternative routes of producing syngas such as partial oxidation and conventional steam reforming (Kumar et al., 2019). Besides CO_2 and CH_4 are the main biogas components hence DRM offers a direct route for biogas upgrading expanding the horizons of this renewable resource (le Saché et al., 2019).

Therefore, extensive efforts have been focused on the development of highly active, thermally stable, economic, and scalable catalysts that will resist deactivation due to sintering and carbon deposition. The general performance of the catalyst towards DRM essentially rests on many factors such as the type of the active metal, nature of the support, surface area, active metal particle size, extent of dispersion, and interaction of the metal particles with the support (Usman et al., 2015). Both noble (Rh, Ru, Pd, and Pt) and transition metals (Ni, Co and Fe) based catalysts (Liu et al., 2009; Joo et al., 2021) have been investigated extensively. Transition metal catalysts, particularly Ni, have attracted attention for industrial scale application due to their low cost and high activity in DRM reaction (Kwon et al., 2021; Bai et al., 2022), however, are highly prone to deactivation by sintering and carbon deposition (Hou et al., 2006). On the other hand, noble metals-based catalysts have proven to exhibit superior resistance to deactivation by carbon deposition and have higher activity and stability than non-noble metals (Jones et al., 2008), but their industrial application is limited by their high cost and gradual deactivation due to sintering. Therefore there is a need to efficiently synthesize noble metals-based catalyst that are more durable for longer reaction period (Ginsburg et al., 2005; Xiao and Xie, 2022). The past few years exsolution has been identified as an alternative method to produce highly active and exceptionally stable catalysts (Kwon et al., 2020; Kousi et al., 2021; Zubenko et al., 2017; Naeem et al., 2020). In this, the desirable active sites are incorporated in a inorganic matrix (i.e., perovskite or pyrochlore oxide) under oxidizing conditions and are subsequently segregated on the surface of the oxide, which now acts as a support, under reducing atmosphere in the form of metallic nanoparticles (Pakhare and Spivey, 2014; Kousi et al., 2021; le Saché et al., 2018; Tang et al., 2019). As these particles are formed from within the support in a disassembly method, they are socketed, thus strained, and crystallographically aligned with the support which endows them with many interesting properties such as thermal stability, coke resistance and high activity (Zhao et al., 2021; Kim et al., 2021; Cheng et al., 2021).

Exsolution of noble metals poses additional challenges as in order to keep the cost low needed to attempt exsolution from very low loadings. This is expected to be very challenging due to thermodynamic and kinetic limitations, since the noble metal would be strongly bound within the perovskite and will not be exsolved easily. Previous studies conducted on dilute noble metals exsolved systems concluded that in order to do so efficiently microstructure, nanostructure and extrinsic conditions' tuning is necessary.

Herein, we efficiently exsolve from dilute noble metal systems using B-site chemistry as a tuning parameter. We introduce a very small amount of a transition metal (Ni) and explore the effect this has on the extent of exsolution and particle characteristics and ultimately in the catalytic activity of the newly designed samples. We demonstrate a series of catalytically active materials but also present a novel method of producing tandem catalysts, which is expected to greatly impact a lot more areas of catalytic research.

2 Materials and methods

2.1 Materials synthesis

Perovskite oxide powders were prepared by a modified solid state synthesis described in detail previously (Tang et al., 2019). In order to ensure strict control of stoichiometry we use a solid-state synthesis preparation method and a Ca-based titanate of the general formula LaCaRh(Ni)TiO_3. We introduce a high degree of A-site vacancies to further promote ion diffusion and as a consequence exsolution, and employ the series of $La_{0.43}Ca_{0.37}Rh_xNi_yTi_{(1-x-y)}O_3$. We synthesize the series members with x = 0.03 and y = 0 and 0.03 (referred to as p-Rh and p-RhNi respectively). To exsolve particles, the samples were reduced at temperature in a controlled atmosphere furnace, under continuous flow of H_2 (100 mL·min^{-1}) at temperatures of 800°C and 1,000°C with a dwell of 10 h with heating and cooling rates of 5°C·min^{-1}. Before the reduction, all samples were pre-treated at room temperature under a flow of 100 mL·min^{-1} argon for 10 min to remove gas impurities in the chamber.

2.2 Materials characterisation

2.2.1 X-ray diffraction

The crystalline phase components of all freshly prepared and reduced samples were investigated using X-ray diffraction (XRD) (X'Pert Powder from PANalytical) with Cu Kα radiation (λ = 0.154 nm) at 40 kV and 30 mA. For the measurements, the diffraction patterns were recorded from 10° to 90° (2θ) with a scanning speed of 0.011°sec·s^{-1}.

2.2.2 Scanning electron microscopy

Scanning electron microscope (SEM) images of the fresh and reduced samples were taken using Thermo Fischer Apreo 2 SEM. The catalyst samples were affixed to the sampling plate with carbon black tape and partially coated with silver to improve the imaging of samples. The SEM images were taken under high vacuum condition with a working distance range of 2.8–10 mm and magnification range of 100 to 1,000,000. Image processing program (ImageJ) was used to carry out the morphological analysis of the SEM images such as crystal size and exsolved particle population and size.

2.2.3 Transmission electron microscopy

Transmission Electron Microscopy (TEM) was carried out on the reduced LaCaRh(Ni)TiO_3 sample using Talos F200I instrument from ThermoFisher with an electron source of 200 kV. To prepare the TEM samples, the powder was dispersed in ethanol in an

ultrasonic bath, dropped onto copper grids coated with lacey carbon film and dried.

2.2.4 Thermogravimetric analysis

Thermogravimetric analysis (TGA) of reduced and spent samples was carried out using TA instruments (SDTQ650 V8.3). For each analysis, 10 mg of sample was introduced into the unit crucible and continuous gas flow of air with a flow rate of 50 mL·min^{-1} was used. A ramping rate of 10°C/min was used to heat each sample from room temperature to 800°C, and subsequently cooled down to room temperature at the same rate.

2.3 Catalytic testing

Catalytic experiments were conducted at atmospheric pressure in a fixed-bed vertical quartz tubular reactor housed inside a tube furnace with a column length of 30 cm, and inner diameter of 1 cm. The gas flow was fed into the top of the tube. The reactor temperature was controlled using a temperature programmed furnace from Carbolite Furnaces, and K-type thermocouple was placed as close to the catalyst bed as possible to accurately monitor the inner temperature. Inlet gas flow rates of reactants were controlled by mass flow controllers (MFCs) from Aalborg, and the effluent dry gas stream was analyzed using an on line gas analyser (ABB AO 2020) equipped with infrared gas detectors for CO_2, CH_4 and CO and a thermal conductivity detector for H_2. H_2O (steam) in the effluent stream was removed in a cold trap by condensation to ensure no water reaches the ABB analyzer. The total flow rate of the effluent streams was measured by a flow meter. For each experiment, 0.1 g of catalyst powder was packed in the quartz tube using quartz wool in such a way that the catalyst powder is uniformly placed on top of the quartz wool. Before the catalytic reaction, the catalyst samples were pre-treated with a flow of H_2 and N_2 gas (5 mL·min^{-1} and 45 mL·min^{-1} respectively) at 600°C, for 1 h, after which the temperature was maintained at 600°C under 75 mL·min^{-1} N_2 flow, until the reaction mixture was introduced. Following the catalyst thermal activation, the reactant gas mixture of (12.5% CH_4: 12.5% CO_2: 75% N_2) with a total flow rate of 50 mL·min^{-1} was introduced to the reactor, giving a gas hourly space velocity (GSHV) of 1,474 h^{-1} and a weight hourly space velocity of 30 L·g^{-1} h^{-1}. The catalytic test was carried out in the temperature range of 600°C–800°C with a temperature increment of 50 °C. The reaction was carried out for 30 min at each temperature.

The following equations were used to determine the values presented in this paper:

$$CH_4\ \text{conversion}\ (\%) = \frac{F_{\text{Total,In}} \times [CH_4]_{in} - F_{\text{Total,Out}} \times [CH_4]_{Out}}{F_{\text{Total,In}} \times [CH_4]_{in}} \times 100 \quad (2)$$

$$CO_2\ \text{conversion}\ (\%) = \frac{F_{\text{Total,In}} \times [CO_2]_{in} - F_{\text{Total,Out}} \times [CO_2]_{Out}}{F_{\text{Total,In}} \times [CO_2]_{in}} \times 100 \quad (3)$$

$$\frac{H_2}{CO} = \frac{F_{H_{2,out}}}{F_{CO_{2,out}}} \quad (4)$$

F_{Total} is the total volumetric flow rate (mL min^{-1}), the brackets indicate the volumetric percentages of the respective gases, and the subscripts in and out refer to inlet and outlet, respectively. The H_2/CO molar flow rate ratio is calculated by the mol of H_2 gas out in to the mol of CO gas in the outlet.

2.4 Thermodynamic simulation

Thermodynamic simulation was performed using Chemstations' ChemCad software (CHEMCAD 7.1.8) to obtain the thermodynamic equilibrium conversions for all the reactants of DRM reaction. The equation of state used was the Soave–Redlich– Kwong. The reactor was simulated as a Gibbs reactor in order to calculate thermodynamic equilibrium limits. The total inlet flow rate and the percentages of the reactants used in the ChemCad simulation were the same as those used in catalytic experiment above.

2.5 Carbon deposition analysis

To examine the carbon deposition during catalytic testing, the tests were followed by temperature programmed oxidation experiments (TPO) in vertical fixed bed packed flow reactor. For these experiments, 30 mg of used sample, were oxidized under a 30 mL·min^{-1} flow of 3% O_2/Ar. The heating program run from 50 to 800°C with a ramp of 10°C·min^{-1} and was stopped when all signals reached baseline. The total amount of carbon was calculated by integrating the CO_2 curves produced during the experiments. Outlet gas analysis was performed with a Omni-Star GSD 320 mass spectrometer and a secondary electron multiplier detector. The following m/z values were tracked during the experiment: 32 (O_2+) 28 (CO+), and 44 (CO_2+). To gain quantitative results, the mass spectrometer was calibrated with gas mixtures of CO_2 and O_2. The CO signal was monitored and was zero in all cases.

3 Results and discussion

3.1 Doping Ni into a Rh-based titanate lattice

As observed in the SEM images (Figures 1B, C) the grains of the perovskite are relatively large ~500 nm which is a direct result of the fact that we have used a solid-state synthesis preparation method which employs relatively high synthesis temperature in order to ensure control over stoichiometry. This is known to hinder exsolution, since ion diffusion to the surface, to form nanoparticles, becomes more difficult. Here we take on board the design principles of previous work done in the area (Tang et al., 2019; Kyriakou et al., 2020) but take these one step further by substituting a small amount of Ni in the perovskite lattice. This is because Ni is known to have high segregation energy and could in principle be able to affect the diffusion of other ions towards the surface during exsolution (Kwon et al., 2017). Therefore, we design two parent materials based on a $CaTiO_3$ perovskite and are $La_{0.43}Ca_{0.37}Rh_{0.03}Ti_{0.97}O_3$ (p-Rh) and $La_{0.43}Ca_{0.37}Rh_{0.03}Ni_{0.03}Ti_{0.94}O_3$ (p-RhNi) (Figure 1). The diffraction patterns of the as prepared p-Rh and p-RhNi (Figure 1A) showed characteristic peaks, almost identical to a

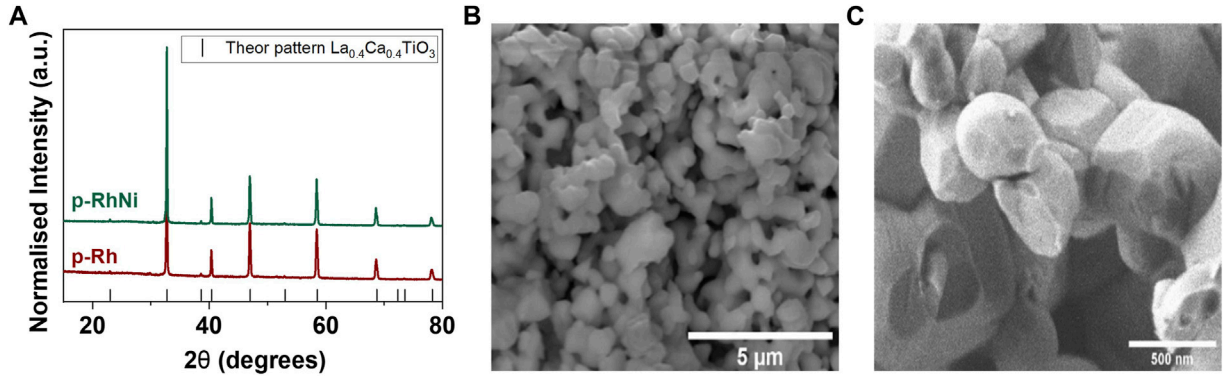

FIGURE 1
Preparing Rh-Ni doped perovskites **(A)** X-ray diffraction spectra of the as-prepared samples $La_{0.43}Ca_{0.37}Rh_{0.03}Ti_{0.97}O_3$ (Rh_3), and $La_{0.43}Ca_{0.37}Rh_{0.03}Ni_{0.03}Ti_{0.94}O_3$ (Rh_3Ni_3). Representative SEM images of the **(B)** micro and **(C)** nanostructure of the as prepared materials.

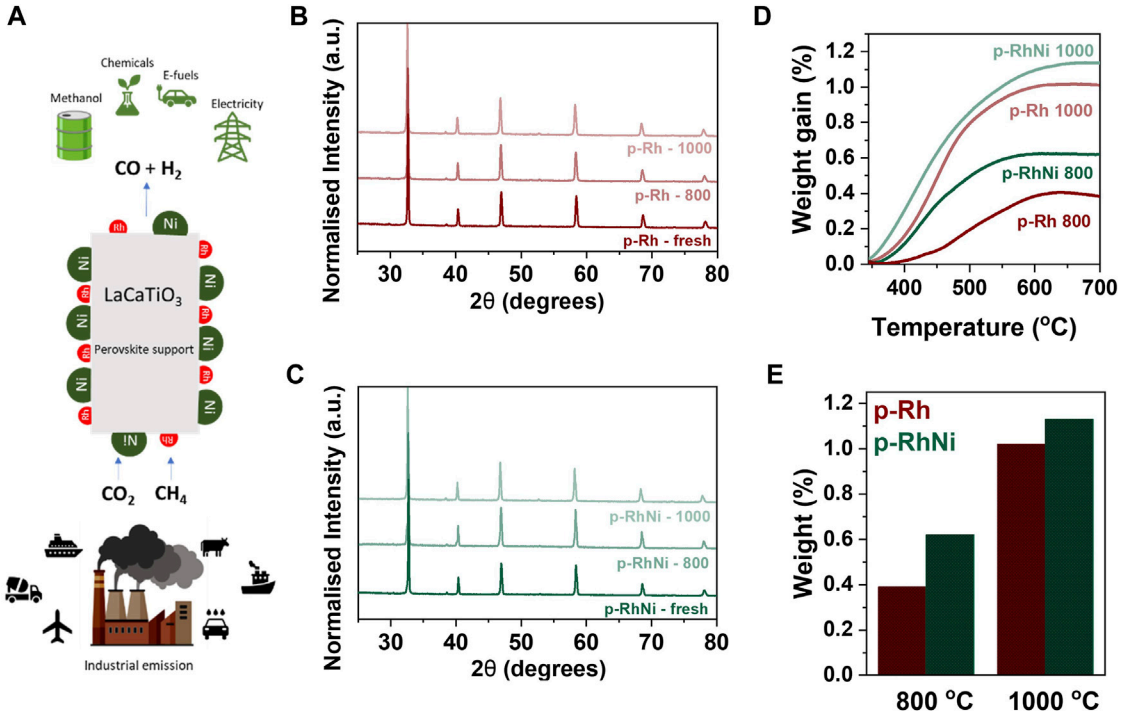

FIGURE 2
Provoking exsolution **(A)** Schematic representation of the concept of this work **(B)** XRD patterns of the undoped sample **(C)** XRD patterns of the Ni-doped samples **(D)** TGA curves of the reduced samples after oxidation **(E)** Quantification of the weight gained during oxidation/TGA experiments.

$LaCaTiO_3$ perovskite (Tang et al., 2019). This indicates that both Rh and Ni cation substitutions were successful despite the fact that the ionic radii of both substitutes, Ni^{2+} (0.69 Å) and Rh^{3+} (0.67 Å) are bigger in value than the native Ti^{4+}(0.61 Å) (Kousi et al., 2021; Royer et al., 2014), they are relatively similar, therefore they were completely soluble in the perovskite lattice. This also implies that the non-stoichiometry A-site deficiency applied did not hinder B-site cation solubility in the perovskite lattice. Interestingly, we can notice a slight shift of all peaks to lower 2θ angles with substitution of the Rh into the $LaCaTiO_3$ which becomes even more prominent with the addition of the Ni cation and can be attributed to the lattice expansion or volume increase caused by the substitution of smaller ionic radii Ti^{4+} with bigger ones. The prepared materials are uniform and have ~500 nm grains making them quite porous (Figure 1B). Overall, the results presented here demonstrate that we have successfully prepared highly porous,

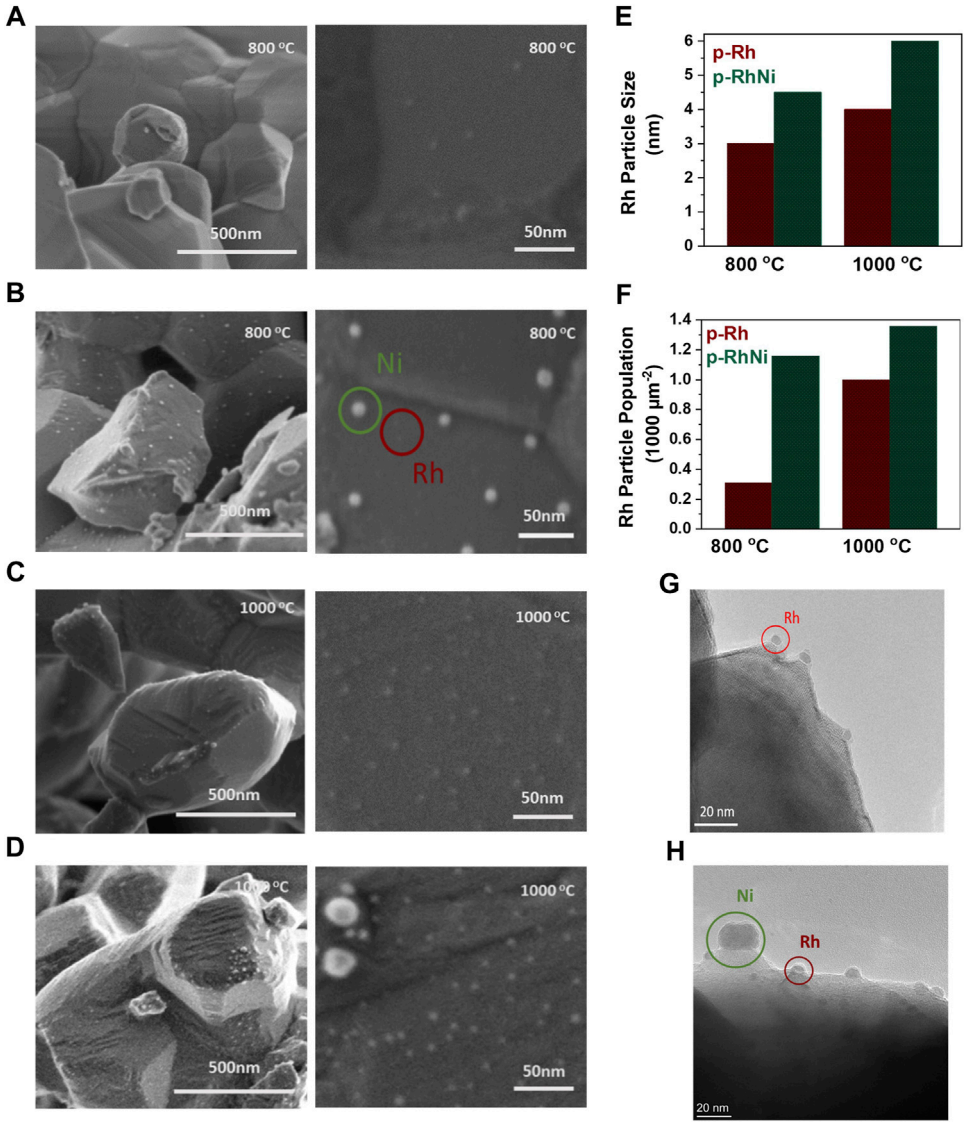

FIGURE 3
Micro and nanostructure of the exsolved catalysts: **(A)** Rh_3 reduced at 800°C **(B)** Rh_3Ni_3 reduced at 800°C **(C)** Rh_3 reduced at 1,000°C **(D)** Rh_3Ni_3 reduced at 1,000°C **(E)** Particle size of the Rh exsolved particles of the reduced catalysts calculated from SEM images **(F)** Population of the Rh exsolved particles of the reduced catalysts calculated from SEM images **(G)** TEM image of Rh_3 **(H)** TEM image of the Rh_3Ni_3.

single phase Rh and Rh-Ni-containing perovskites that will be used to efficiently prepare low-cost noble metal catalysts for the conversion of greenhouse gases to useful products.

3.2 Exsolution of Rh nanoparticles

In order to exsolve metallic particles on the surface of the perovskite, temperature and dwell time are important in order to allow for the diffusion of the cations towards the surface, hence the samples were reduced at 800 and 1,000°C for 10 h respectively (Figure 2). This is consistent with previous studies that use similar temperature and dwell time to provoke exsolution in such systems (Tang et al., 2019; Otto et al., 2019). SEM imaging was used to study the morphology, particle size, population, and dispersion of the exsolved nanoparticles of p-Rh and p-RhNi samples (Figure 3) reduced at 800°C and 1,000°C. The average exsolved Rh particle sizes for p-Rh and p-RhNi reduced at 800°C were 3 and 4.5 nm respectively. In contrast, the average exsolved Rh particle sizes reduced at 1,000 °C were 4 nm for p-Rh and 6 nm for p-RhNi. The population difference, however, was even more prominent with ~300 p μm^{-2} and ~1,200 p μm^{-2} for p-Rh and p-RhNi at 800°C respectively and ~1,000 p μm^{-2} and ~1,400 p μm^{-2} respectively at 1000°C. For the p-RhNi sample reduced at 800°C and 1,000 °C, the mean Ni particle sizes was measured at ~15 nm and 104 p μm^{-2} at 800°C, however the size varied a lot at 1,000°C (Figures 3A–F). The two particles are exsolved separately and not as alloys as seen in Figures 3G, H (Xu et al., 2020). This is very important because it paves the way to the design and

preparation of materials that will fulfill the so-called tandem catalysis concept, as two completely separate active sites are available on the surface in one step.

3.2.1 Effect of temperature on the exsolution of Rh nanoparticles

The increase in the particle size and population with temperature in exsolution is expected as increase in temperature results in an increase in ion diffusion; as a result more Rh and Ni particles migrate to the surface provoking nucleation and/or joining the already exsolved particles (Kousi et al., 2021; Tang et al., 2019; Gao et al., 2016). Overall, at low temperature, the results are expected to follow the nucleation theory. This theory suggests that at low temperature nucleation (population growth) is favored rather than particle size growth, a trend that flips as the temperature increases (Tang et al., 2019; Gao et al., 2016). However, the population here increases as reduction temperature changes from 800°C to 1,000°C seemingly contradicting the nucleation/growth theory. This may be due to fact that, at 800°C, the temperature is insufficient for extensive Rh exsolution due to the dilute substitution of the cations in the titanate oxide lattice. Similar results have been reported previously, however as compared to previous studies the particle size seems to be higher than the ones reported for similar materials (Tang et al., 2019), indicating the effect of the second metal and/or the overall environment of exsolution (5% H_2 vs. 100% H_2).

3.2.2 Effect of Ni substitution on the exsolution of Rh nanoparticles

In order to identify the effect of Ni substitution in the extent of Rh exsolution, the XRD and SEM results obtained for reduced samples were compared. When monitoring the p-Rh and p-RhNi samples reduced at the same temperature, it is evident that both the population and size of the Rh exsolved particles is enhanced in the presence of Ni. This enhancement in the Rh exsolution can be explained in terms of segregation energies of each B-site species: it has been reported that in the multiple B-site cation system, introducing more reducible ions would lower the segregation energy (Tang et al., 2021; Tang et al., 2019; Guo et al., 2022). Generally, Rh has a very negative Gibbs free energy of reduction and thus normally reduces at around 300°C (Tang et al., 2019). However, being substituted into the titanate lattice in such dilute amounts, its reduction temperature is 'increased' due to the strong interaction with the lattice, hence the reason fewer Rh particles were exsolved in p-Rh sample reduced at 800°C (Figure 3A). In principle, in the bimetallic system, the substitution of Ti with Ni which has lower Gibbs energy of reduction (Guo et al., 2022) could decrease the energy and therefore the temperature required to exsolve the Rh from the bulk of the perovskite thus leading to higher particle size and population. Additionally, it has been reported that the oxygen vacancies in the perovskite lattice highly improve the exsolution of B-site cations (Kousi et al., 2021; (Tang et al., 2019; Neagu et al., 2013; Neagu et al., 2015; Neagu et al., 2017; Tang et al., 2021; Guo et al., 2022). The B-site substitution of higher valence cation (Ti^{4+}) with a cation of lower valence (Ni^{2+}) results in decrease in oxygen stoichiometry as the perovskite compensates for the decrease in the average B-site charge. Subsequently, after substitution, the already A-site deficient perovskite also becomes more oxygen deficient. These oxygen vacancies introduced by the substitution of a lower oxidation state B-site cation as compared to Ti (along with the oxygen vacancies introduced upon reducing) destabilizes the perovskite lattice in a greater extent and thus are thought to increase spontaneous exsolution of Rh, as it tries to re-establish A-site stoichiometry (Neagu et al., 2013; Guo et al., 2022). One more thing that is prominent in these samples is the fact that the Rh particles exsolved near the Ni particles appear to be bigger than those away from the Ni particles which is consistent with the previous studies. Nevertheless, as demonstrated in Figures 2D, E, thermogravimetric analysis verifies the overall trend that indeed temperature has a greater effect on exsolution than the addition of the second metal, since the increase in temperature of reduction by 200°C leads to a much larger oxygen uptake which implies much higher degree of exsolution.

3.3 Catalytic activity

The results of the catalytic activity tests, in terms of conversion of CH_4 and CO_2, H_2/CO ratio are presented in Figure 4. All prepared catalysts were active for dry reforming of methane except for the p-Rh sample reduced at 800°C, which is attributed to the insufficient number of active sites available to convert the reactant stream. It was also evident that the CO_2 conversion was almost always higher than that of CH_4. This is due to the reverse water gas shift reaction (RWGS), which also consumes CO_2, and occurs in parallel with the dry reforming of methane, keeping the H_2/CO product ratio for most part below unity (Figure 4).

3.3.1 Effect of reduction temperature on catalyst activity

To investigate the effect of reduction temperature on the catalyst's performance, a comparison of the activity of the p-Rh and p-RhNi catalyst reduced at 800°C with those reduced at 1,000°C was made (Figure 4). It was evident that, in general, p-Rh and p-RhNi samples reduced at 1,000°C showed the best catalytic performance for dry reforming of methane reaction. As mentioned earlier, the p-Rh sample reduced at 1,000°C formed much bigger nanoparticles and in higher number as compared to the sample reduced at 800°C (Figure 3) which were almost non-existent which is what is probably the governing factor for the latter's very low activity. The p-Rh sample reduced at 1,000°C is indeed much more active, even reaching ~70% CO_2 conversion for the highest temperature as compared to the 800°C reduced samples which was practically zero. For the p-RhNi catalyst, the activity seems to be fairly similar for the two samples reduced at 800°C and 1,000°C, however, the 1,000°C reduced sample is more active at higher temperatures (>700°C). That could be attributed to the greater amount of Ni and Rh particles on the surface of that sample, probably with a focus on the Ni particles as Figure 5 indicates the existence of slightly higher carbon deposition probably owning to the existence of bigger Ni particles. It is interesting that although the 800°C reduced sample has a lower population (and size) of Rh exsolved nanoparticles, its reactivity is fairly similar to its 1,000°C reduced counterpart. This could be attributed to the fact that the Ni particles were much bigger at 1,000°C and more scarce which has been known to be a determining

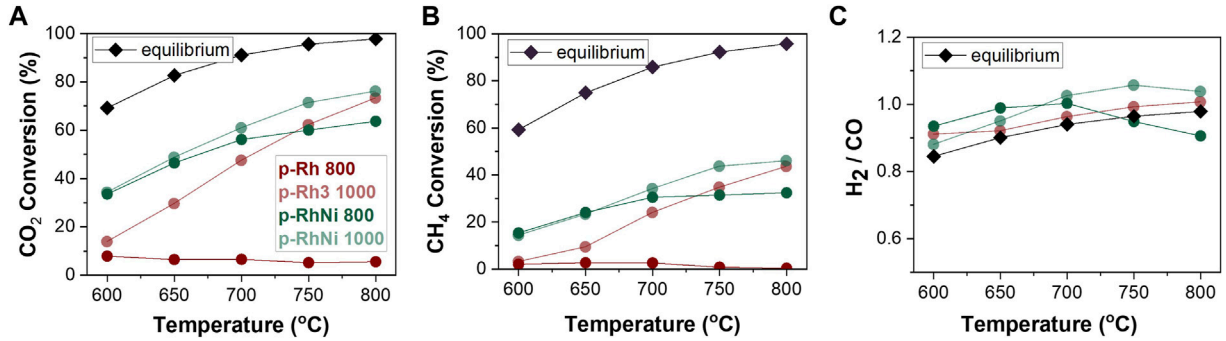

FIGURE 4
Catalytic activity: **(A)** CO_2 conversion, **(B)** CH_4 conversion **(C)** H_2/CO ratio.

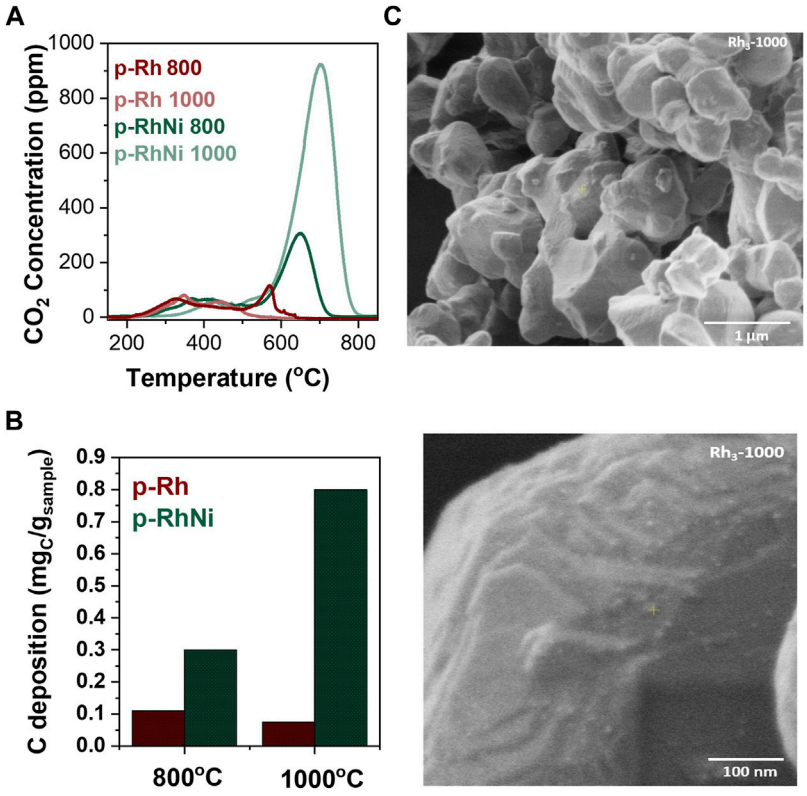

FIGURE 5
After testing characterization **(A)** Temperature Programmed Oxidation **(B)** Carbon deposition quantification **(C)** SEM images of the materials after testing representative for all samples.

factor of the activity in DRM (Lu et al., 2021). However, the Rh population in the 1,000°C sample is indeed larger overall which makes it more active at the higher temperature range.

3.3.2 Effect of Ni doping on catalyst activity

To understand the crucial role of Ni substitution on the catalyst performance, we compared the p-Rh and p-RhNi samples reduced at the same temperature. The results shown in Figure 4 demonstrate that there is a significant enhancement in catalytic activity for the samples that are indeed Ni dopped. When comparing the catalyst performance of p-RhNi and p-Rh reduced at the same temperature (800°C), the p-RhNi catalyst achieved the highest CH_4 and CO_2 conversion (~33 and 65% respectively), whereas there were practically no particles in the p-Rh sample reduced at 800°C. The enhanced activity of p-RhNi can be directly attributed to the high population of active Rh particles on the surface of the perovskite

induced by the substitution of Ni as well as combined population of Rh and Ni particles (Kousi et al., 2021; Tang et al., 2019; Neagu et al., 2013). For the case of the 1,000°C reduced samples the Ni doped catalyst is overall ~20% more active almost throughout the temperature range. Interestingly the samples seem to get similar conversions at the highest temperature tested both for CH_4 and CO_2. This could be attributed to the fact that the total amount of metal originally doped in the sample is indeed too low (~1%) and they are both experiencing such limitations.

3.3.3 After testing characterization

Samples were characterized after testing using temperature programmed oxidation and SEM analysis (Figure 5). Figures 5A, B show the amount of carbon deposition on the surface of the materials. It is evident that the nickel doped samples do contain higher amount of carbon deposition than the original Rh catalysts which is expected as noble metals are very resistant to any sort of carbon deposition. As expected, the Ni doped sample that had the higher overall conversion also contained the largest Ni particle size and demonstrated the highest amount of carbon deposition. However, overall, as these are samples produced by the exsolution method the amount of carbon quantified is minimal ranging from 0.02 to 0.9 mg_C/mg_{Sample} which is the orders of magnitude less than other infiltrated samples tested for similar reactions (Vasiliades et al., 2018). This is also evident by the SEM images (Figure 5C). The images were taken after catalytic testing and are characteristic of the whole surface of the materials. The nano and microstructure of the materials seem intact with no signs of surface degradation of carbon deposition.

4 Conclusion

In this work, an A-site deficient Rh containing perovskite was doped with a minor amount of Ni in order to monitor its effect on exsolution of metallic nanoparticles on the surface of the oxide and its spillover effect on the catalytic activity of the materials. Normally, Rh being incorporated in tiny quantities in the perovskite lattice is quite stable and therefore limited to exsolve. We conclude that the doping of Ni could indeed enhance its exsolution capabilities driving more Rh particles towards the surface of the perovskite. Indeed, the p-RhNi perovskites also demonstrated significantly improved catalytic activity in DRM reaction compared with its p-Rh counterparts reduced at the same temperature. However, temperature still seems to be a greater driving force for exsolution of cations from a perovskite lattice. Nevertheless, we demonstrated that there might be a way to produce catalysts with distinct active sites that could be employed for what we normally call tandem catalysis. These materials are produced in a single step and could avoid any deactivation mechanisms usually caused by the degradation of two or more catalysts put together in an assembly method.

Data availability statement

The original contributions presented in the study are publicly available. This data can be found here: https://doi.org/10.15126/surreydata.900627.

Author contributions

MS, SA, L-PM, and SS performed the samples pre-treatment, characterisation and catalytic testing and analysis of the data. AI, assisted with SEM acquisition and interpretation, MS, and SA, wrote the initial draft of the paper, DN designed and fabricated the initial materials, TR and MD contributed to the data interpretation and manuscript refinement. KK conceived the idea of this study, secured the funding for the project, supervised the research, and drafted the final paper. All the authors discussed the results and commented on the manuscript.

Acknowledgments

The authors acknowledge the funding received from the University of Surrey for the APC.

Conflict of interest

The authors declare that the research was conducted in the absence of any commercial or financial relationships that could be construed as a potential conflict of interest.

Publisher's note

All claims expressed in this article are solely those of the authors and do not necessarily represent those of their affiliated organizations, or those of the publisher, the editors and the reviewers. Any product that may be evaluated in this article, or claim that may be made by its manufacturer, is not guaranteed or endorsed by the publisher.

References

Abdulrasheed, A., Jalil, A. A., Gambo, Y., Ibrahim, M., Hambali, H. U., and Shahul Hamid, M. Y. (2019). A review on catalyst development for dry reforming of methane to syngas: Recent advances. *Renew. Sustain. Energy Rev.* 108, 175–193. doi:10.1016/j.rser.2019.03.054

Ainsworth, E. A., Rogers, A., and Leakey, A. D. B. (2008). Targets for crop biotechnology in a future high-CO2 and high-O3 world. *Plant Physiol.* 147, 13–19. doi:10.1104/pp.108.117101

Bai, Y., Sun, K., Wu, J., Zhang, M., Zhao, S., Kim, Y. D., et al. (2022). The Ga-promoted Ni/CeO2 catalysts for dry reforming of methane with high stability induced by the enhanced CO2 activation. *Mol. Catal.* 530, 112577. doi:10.1016/j.mcat.2022.112577

Buelens, L. C., Galvita, V. V., Poelman, H., Detavernier, C., and Marin, G. B. (2016). Super-dry reforming of methane intensifies CO2 utilization via Le Chatelier's principle. *Science* 354, 449–452. doi:10.1126/science.aah7161

Cheng, F., Duan, X., and Xie, K. (2021). Dry reforming of CH4/CO2 by stable Ni nanocrystals on porous single-crystalline MgO monoliths at reduced temperature. *Angew. Chem.* 133, 18940–18947. doi:10.1002/ange.202106243

Gao, J., Hou, Z., Lou, H., and Zheng, X. (2011). "Chapter 7 - dry (CO2) reforming," in *Fuel cells: Technologies for fuel processing*. Editors D. Shekhawat, J. J. Spivey, and D. A. Berry (Amsterdam: Elsevier), 191–221. doi:10.1016/B978-0-444-53563-4.10007-0

Gao, Y., Chen, D., Saccoccio, M., Lu, Z., and Ciucci, F. (2016). From material design to mechanism study: Nanoscale Ni exsolution on a highly active A-site deficient anode material for solid oxide fuel cells. *Nano Energy* 27, 499–508. doi:10.1016/j.nanoen.2016.07.013

Ginsburg, J. M., Piña, J., El Solh, T., and de Lasa, H. I. (2005). Coke Formation over a nickel catalyst under methane dry reforming conditions: Thermodynamic and kinetic models. *Ind. Eng. Chem. Res.* 44, 4846–4854. doi:10.1021/ie0496333

Guo, J., Cai, R., Cali, E., Wilson, G. E., Kerherve, G., Haigh, S. J., et al. (2022). Low-temperature exsolution of Ni–Ru bimetallic nanoparticles from A-site deficient double perovskites. *Small* 18, 2107020. doi:10.1002/smll.202107020

Hou, Z., Chen, P., Fang, H., Zheng, X., and Yashima, T. (2006). Production of synthesis gas via methane reforming with CO22 on noble metals and small amount of noble-(Rh-) promoted Ni catalysts. *Int. J. Hydrog. Energy* 31, 555–561. doi:10.1016/j.ijhydene.2005.06.010

Izquierdo, U., Barrio, V. L., Requies, J., Cambra, J. F., Güemez, M. B., and Arias, P. L. (2013). Tri-reforming: A new biogas process for synthesis gas and hydrogen production. *Int. J. Hydrog. Energy* 38, 7623–7631. doi:10.1016/j.ijhydene.2012.09.107

Jones, G., Jakobsen, J. G., Shim, S. S., Kleis, J., Andersson, M. P., Rossmeisl, J., et al. (2008). First principles calculations and experimental insight into methane steam reforming over transition metal catalysts. *J. Catal.* 259, 147–160. doi:10.1016/j.jcat.2008.08.003

Joo, S., Kim, K., Kwon, O., Oh, J., Kim, H. J., Zhang, L., et al. (2021). Enhancing thermocatalytic activities by upshifting the d-band center of exsolved Co-Ni-Fe ternary alloy nanoparticles for the dry reforming of methane. *Angew. Chem. Int. Ed.* 60, 15912–15919. doi:10.1002/anie.202101335

Kim, H., Lim, C., Kwon, O., Oh, J., Curnan, M. T., Jeong, H. Y., et al. (2021). Unveiling the key factor for the phase reconstruction and exsolved metallic particle distribution in perovskites. *Nat. Commun.* 12, 6814. doi:10.1038/s41467-021-26739-1

Kousi, K., Tang, C., Metcalfe, I. S., and Neagu, D. (2021). Emergence and future of exsolved materials. *Small* 17, 2006479. doi:10.1002/smll.202006479

Kumar, N., Kanitkar, S., Wang, Z., Haynes, D., Shekhawat, D., and Spivey, J. J. (2019). Dry reforming of methane with isotopic gas mixture over Ni-based pyrochlore catalyst. *Int. J. Hydrog. Energy* 44, 4167–4176. doi:10.1016/j.ijhydene.2018.12.145

Kwon, O., Sengodan, S., Kim, K., Kim, G., Jeong, H. Y., Shin, J., et al. (2017). Exsolution trends and co-segregation aspects of self-grown catalyst nanoparticles in perovskites. *Nat. Commun.* 8, 15967. doi:10.1038/ncomms15967

Kwon, O., Joo, S., Choi, S., Sengodan, S., and Kim, G. (2020). Review on exsolution and its driving forces in perovskites. *J. Phys. Energy* 2, 032001. doi:10.1088/2515-7655/ab8c1f

Kwon, O., Huang, R., Cao, T., Vohs, J. M., and Gorte, R. J. (2021). Dry reforming of methane over Ni supported on LaMnO3 thin films. *Catal. Today* 382, 142–147. doi:10.1016/j.cattod.2021.08.001

Kyriakou, V., Neagu, D., Zafeiropoulos, G., Sharma, R. K., Tang, C., Kousi, K., et al. (2020). Symmetrical exsolution of Rh nanoparticles in solid oxide cells for efficient syngas production from greenhouse gases. *ACS Catal.* 10, 1278–1288. doi:10.1021/acscatal.9b04424

le Saché, E., Pastor-Pérez, L., Watson, D., Sepúlveda-Escribano, A., and Reina, T. R. (2018). Ni stabilised on inorganic complex structures: Superior catalysts for chemical CO2 recycling via dry reforming of methane. *Appl. Catal. B Environ.* 236, 458–465. doi:10.1016/j.apcatb.2018.05.051

le Saché, E., Johnson, S., Pastor-Pérez, L., Amini Horri, B., and Reina, T. R. (2019). Biogas upgrading via dry reforming over a Ni-Sn/CeO2-Al2O3 catalyst: Influence of the biogas source. *Energies* 12, 1007. doi:10.3390/en12061007

le Saché, E., and Reina, T. R. (2022). Analysis of Dry Reforming as direct route for gas phase CO2 conversion. The past, the present and future of catalytic DRM technologies. *Prog. Energy Combust. Sci.* 89, 100970. doi:10.1016/j.pecs.2021.100970

Liu, D., Quek, X. Y., Cheo, W. N. E., Lau, R., Borgna, A., and Yang, Y. (2009). MCM-41 supported nickel-based bimetallic catalysts with superior stability during carbon dioxide reforming of methane: Effect of strong metal–support interaction. *J. Catal.* 266, 380–390. doi:10.1016/j.jcat.2009.07.004

Lu, Y., Guo, D., Zhao, Y., Zhao, Y., Wang, S., and Ma, X. (2021). Enhanced performance of xNi@yMo-HSS catalysts for DRM reaction via the formation of a novel SiMoOx species. *Appl. Catal. B Environ.* 291, 120075. doi:10.1016/j.apcatb.2021.120075

Maestri, M., Vlachos, D. G., Beretta, A., Groppi, G., and Tronconi, E. (2009). A C1 microkinetic model for methane conversion to syngas on Rh/Al2O3. *AIChE J.* 55, 993–1008. doi:10.1002/aic.11767

McCarthy, J. J., Canziani, O. F., Leary, N. A., Dokken, D. J., and White, K. S.climat, G. d'experts intergouvernemental sur l'évolution du, II, I. P. on C. C. W. G., Change, I. P. on C., and Science, I. P. on C. C. W. G. (2001). *Climate change 2001: Impacts, adaptation, and vulnerability: Contribution of working group II to the third assessment report of the intergovernmental panel on climate change*. Cambridge University Press.

Naeem, M. A., Abdala, P. M., Armutlulu, A., Kim, S. M., Fedorov, A., and Müller, C. R. (2020). Exsolution of metallic Ru nanoparticles from defective, fluorite-type solid solutions $Sm_2Ru_xCe_{2-x}O_7$ to impart stability on dry reforming catalysts. *ACS Catal.* 10, 1923–1937. doi:10.1021/acscatal.9b04555

Naidja, A., Krishna, C. R., Butcher, T., and Mahajan, D. (2003). Cool flame partial oxidation and its role in combustion and reforming of fuels for fuel cell systems. *Prog. Energy Combust. Sci.* 29, 155–191. doi:10.1016/S0360-1285(03)00018-2

Neagu, D., Tsekouras, G., Miller, D. N., Ménard, H., and Irvine, J. T. S. (2013). *In situ* growth of nanoparticles through control of non-stoichiometry. *Nat. Chem.* 5, 916–923. doi:10.1038/nchem.1773

Neagu, D., Oh, T.-S., Miller, D. N., Ménard, H., Bukhari, S. M., Gamble, S. R., et al. (2015). Nano-socketed nickel particles with enhanced coking resistance grown *in situ* by redox exsolution. *Nat. Commun.* 6, 8120. doi:10.1038/ncomms9120

Neagu, D., Papaioannou, E. I., Ramli, W. K. W., Miller, D. N., Murdoch, B. J., Ménard, H., et al. (2017). Demonstration of chemistry at a point through restructuring and catalytic activation at anchored nanoparticles. *Nat. Commun.* 8, 1855. doi:10.1038/s41467-017-01880-y

Otto, S.-K., Kousi, K., Neagu, D., Bekris, L., Janek, J., and Metcalfe, I. S. (2019). Exsolved nickel nanoparticles acting as oxygen storage reservoirs and active sites for redox CH4 conversion. *ACS Appl. Energy Mat.* 2, 7288–7298. doi:10.1021/acsaem.9b01267

Pakhare, D., and Spivey, J. (2014). A review of dry (CO 2) reforming of methane over noble metal catalysts. *Chem. Soc. Rev.* 43, 7813–7837. doi:10.1039/C3CS60395D

Royer, S., Duprez, D., Can, F., Courtois, X., Batiot-Dupeyrat, C., Laassiri, S., et al. (2014). Perovskites as substitutes of noble metals for heterogeneous catalysis: Dream or reality. *Chem. Rev.* 114, 10292–10368. doi:10.1021/cr500032a

Tang, C., Kousi, K., Neagu, D., Portolés, J., Papaioannou, E. I., and Metcalfe, I. S. (2019). Towards efficient use of noble metals via exsolution exemplified for CO oxidation. *Nanoscale* 11, 16935–16944. doi:10.1039/C9NR05617C

Tang, C., Kousi, K., Neagu, D., and Metcalfe, I. S. (2021). Trends and prospects of bimetallic exsolution. *Chem. – Eur. J.* 27, 6666–6675. doi:10.1002/chem.202004950

Usman, M., Wan Daud, W. M. A., and Abbas, H. F. (2015). Dry reforming of methane: Influence of process parameters—a review. *Renew. Sustain. Energy Rev.* 45, 710–744. doi:10.1016/j.rser.2015.02.026

Vasiliades, M. A., Djinović, P., Davlyatova, L. F., Pintar, A., and Efstathiou, A. M. (2018). Origin and reactivity of active and inactive carbon formed during DRM over Ni/Ce0.38Zr0.62O2-δ studied by transient isotopic techniques. *Catal. Today* 299, 201–211. doi:10.1016/j.cattod.2017.03.057

Wang, Y., Yao, L., Wang, S., Mao, D., and Hu, C. (2018). Low-temperature catalytic CO2 dry reforming of methane on Ni-based catalysts: A review. *Fuel Process. Technol.* 169, 199–206. doi:10.1016/j.fuproc.2017.10.007

Xiao, Y., and Xie, K. (2022). Active exsolved metal–oxide interfaces in porous single-crystalline ceria monoliths for efficient and durable CH4/CO2 reforming. *Angew. Chem. Int. Ed.* 61, e202113079. doi:10.1002/anie.202113079

Xu, S., Li, Z., Chu, K., Yao, G., Xu, Y., Niu, P., et al. (2020). NiRu nanoparticles encapsulated in a nitrogen-doped carbon matrix as a highly efficient electrocatalyst for the hydrogen evolution reaction. *Dalton Trans.* 49, 13647–13654. doi:10.1039/D0DT02961K

Zhao, J., Bao, J., Yang, S., Niu, Q., Xie, R., Zhang, Q., et al. (2021). Exsolution–dissolution of supported metals on high-entropy $Co_3MnNiCuZnO_x$: Toward sintering-resistant catalysis. *ACS Catal.* 11, 12247–12257. doi:10.1021/acscatal.1c03228

Zubenko, D., Singh, S., and Rosen, B. A. (2017). Exsolution of Re-alloy catalysts with enhanced stability for methane dry reforming. *Appl. Catal. B Environ.* 209, 711–719. doi:10.1016/j.apcatb.2017.03.047